CrystEngComm

Accepted Manuscript

ROYAL SOCIETY OF CHEMISTRY

www.rsc.org/crystengcomm

CrystEngComm RSCPublishing

ARTICLE

Formation of Rh frame nanorods using Au nanorods as sacrificial template

Cite this: DOI: 10.1039/x0xx00000x

Masaharu Tsuji,*[a,b,c] Yukinori Nakashima,[b] Atsuhiko Yajima[c] and Masashi Hattori[a]

Received 00th January 2012,
Accepted 00th January 2012

DOI: 10.1039/x0xx00000x

www.rsc.org/

This report describes a new formation process of Rh frame structures using Au nanorods (NRs) as sacrificial template. Initially, Au@Rh NRs were prepared by reducing Rh^{3+} in the presence of Au NRs, ascorbic acid, and cetyl trimethyl ammonium bromide (CTAB) in an aqueous solution. After formation of Au@Rh NRs having island type of Rh shells, Rh NR frames, which consist of four side edges and top and bottom edges of NRs, were formed in one step through selective oxidative etching of an Au NR core and Rh shells over such unstable facets as {2 5 0} or {5 12 0} by X^-(X=Br, Cl) + O_2. An alternative method for the formation of Rh NR frame was separation between the formation process of Au@Rh NRs and Rh NR frame by oxidative etching. In this two-step process, after formation of Au@Rh NRs, a similar shape of Rh NR frame having {100} facets as major planes was prepared by the addition of HCl. No Rh frame structure was formed from decahedral Au@Rh particles because smooth Rh shells without interspace were formed: Rh shells over low-index {111} facets were not etched by X^-(X=Br, Cl) + O_2. Results obtained from this study suggest a novel method for the formation of frame structure and constitute new information related to its formation mechanism.

Introduction

In recent years, metallic hollow nanostructures have received great attention because they exhibit unique surface plasmonic and catalytic properties that differ from those of non-hollow nanostructures, and which are superior to them in some cases.[1–5] The most popular technique for generation of such metallic hollow nanostructures with scalable hollow interior and porous walls is galvanic replacement (GR) reactions. We recently studied the syntheses of Ag–Au, Ag–Pd, and Ag–Pt alloy triangular nanoframes in an aqueous solution using GR reactions of Ag nanoprisms with $HAuCl_4$, Na_2PdCl_4, and H_2PtCl_6.[6,7] Their growth mechanisms were examined by observing transmission electron microscopic (TEM), TEM-energy dispersed X-ray spectroscopic (EDS), XRD, and ultraviolet (UV)-visible (Vis)-near infrared (NIR) extinction spectral data. There are a few reports on the formation of nanoframes using metallic nanorods (NRs) and nanowires as sacrificial templates.[8–10]

It is possible to prepare Au, Pd, or Pt rich nanoframes using Ag nanoparticles via sacrifice of an Ag template because the standard electrode potential of Ag^+ (0.7996 eV) is lower than those of $AuCl_4^-$ (1.002 eV), Pd^{2+} (0.951 eV), and $PtCl_6^{2-}$ (1.44 eV). For Rh^{3+}, with a low standard potential of 0.758 eV, it is not easy to find appropriate template metals to form hollow structures using GR reaction. This study demonstrates a simple new synthesis method of forming rod-type Rh nanoframes using Au@Rh NRs as a sacrificial template at the low temperature of 95 °C in an aqueous solution. We use a selective dissolution of Au NRs and Rh to form such hollow structures. The effects of each reagent on the formation of Rh NR nanoframes are studied. To assess the effects of the template shape, we also attempted to prepare frame structures using decahedral Au particles as a template. Based on such data, the growth mechanisms of Rh NR nanoframes are discussed.

Experimental

Materials and experimental procedures

For use in this study, diethylene glycol (DEG: >99.5%), $HAuCl_4{\cdot}4H_2O$ (>99.0%), $RhCl_3{\cdot}3H_2O$ (>99.0%), L(+)-ascorbic acid (>99.5%), cetyl trimethyl ammonium bromide (CTAB) (>99.0%), NaOH (>98%), distilled H_2O (for HPLC level), 10% HCl in water, and C_2H_5OH (>99.5%) were purchased from Kishida Chemical Co. Ltd. All reagents were used without further purification. Gold NRs in an aqueous solution involving CATB, which were prepared using a photochemical method,[11] were supplied by Dai Nippon Toryo Co., Ltd. The aspect ratio

of the gold NRs was about 5 (50 nm length, 10 nm diameter; W4 type).

The Rh shells were overgrown on Au NRs by reduction of $RhCl_3 \cdot 3H_2O$ in an aqueous solution in the presence of CTAB and ascorbic acid. In a typical synthesis, 1.33 mL of Au NRs involving 1.5 mM Au atoms in an aqueous solution, 1 mL of 10 mM $RhCl_3 \cdot 3H_2O$ solution were added to 13 mL of aqueous solution involving 264 mM of CTAB. The Rh/Au molar ratio was 5 for the preparation of Au@Rh NRs. Then, 4 mL of 7.5 mM ascorbic acid was injected into the solution described above using a syringe pump at an injection rate of 33 μL/min. It took 121 min to inject all of the ascorbic acid solution. The reagent solution was kept at 95 °C for 3 h under continuous stirring. The final concentrations of Au atoms in Au NRs, $RhCl_3$, CTAB, and ascorbic acid were, respectively, 0.1, 0.5, 178, and 1.55 mM. When the effects of concentrations of ascorbic acid and CTAB were ascertained, their initial concentrations were changed. Then 6 mL of 5% HCl was added after the formation of Au@Rh NRs to study the effects of Cl^- ions. Then the product solution was sampled after heating for various reaction times. When we examine whether Au NRs used for this study are dissolved by the addition of Cl^- ions or not, Au NRs, CTAB, and ascorbic acid with the same concentrations as those described above were dissolved in 20 mL of aqueous solution at 95 °C. Then 6 mL of 5% HCl was added.

DEG was used as both a reductant and solvent for the decahedral Au core seed preparation.[12,13] In the process, 2 g of PVP (MW = 55 k) solution was dissolved in 25 mL DEG and heated to 230 °C in the oil bath. Then 20 mg of $HAuCl_4 \cdot 4H_2O$ in 2 mL DEG was added to the solution above, which was heated at 230 °C for 10 min. The final respective concentrations of $HAuCl_4 \cdot 4H_2O$ and PVP in DEG were 1.8 and 670 mM. After centrifugal separation, Au seeds were redispersed in 24.3 mL aqueous solution. Decahedral Au@Rh particles were prepared using a similar method to that used for the preparation of Au@Rh NRs. 1 mL of 2 mM Au seeds and 1 mL of 20 mM $RhCl_3 \cdot 3H_2O$ solution were added to 13 mL of aqueous solution involving 264 mM of CTAB at 95 °C. 7 mL of 40 mM NaOH was added to the reagent solution to keep the pH value to be 7. Then 4 mL of 7.5 mM ascorbic acid was injected into the reagent solution using a syringe pump. Finally 6 mL of 5% HCl was added to form frame structures. When we examine whether decahedral Au nanoparticles are dissolved by the addition of Cl^- ions or not, decahedral Au seeds, CTAB, and ascorbic acid with the same concentrations as those described above were dissolved in 25 mL of aqueous solution at 95 °C. Then 6 mL of 5% HCl was added.

Characterization of nanoparticles

For TEM and TEM–EDS (200 kV, JEM-2100F; JEOL) observations, Au, Au@Rh, and Rh-rich Rh NR frames were obtained by centrifuging the colloidal solution three times at 15,000 rpm for 30 min. The XRD patterns of the samples were measured using Cu Kα radiation operating at 45 kV and 200 mA (SmartLab; Rigaku Corp.) or operating at 50 kV and 300 mA (RINT-TTR III; Rigaku Corp.). Extinction spectra of the product solutions were measured in the 300–1200 nm region using a spectrometer (UV-3600; Shimadzu Corp.).

Results and discussion

Au@Rh NRs and Rh nanoframes produced from Au NRs as templates

Fig. 1a–1e portray the change in morphology that occurred when Rh^{3+} was reduced over the Au NRs for 3–12 h. At 3 h, Au NRs are covered by many small island-type particles. It is noteworthy that at 6 h, the Rh shells become slightly smooth. Some hollow parts appear in the Au NR core part. At 9 h and 12 h, Au@Rh NRs change to nanoframe structures in most cases. To examine what metals take part in these morphology changes, TEM–EDS images at 3 h and 12 h (Fig. 2a1–2d1 and 2a2–2d2). Results obtained at 3 h show that Au NRs are covered by island-type Rh shells. Frame structures obtained at 12 h predominantly consist of an Rh component and a small Au component remaining at the tip parts of Au NRs in some cases. No evidence of the formation of Au–Rh alloy shells or of Au-Rh alloy nanoframes was observed in these EDS data. The wall thickness of Rh nanoframes was estimated to be 2.4±0.4 nm from TEM images.

Our simple experiments were able to prepare unique Rh frame NRs, but their growth mechanism remains unknown. Therefore, we attempted to clarify the formation mechanism of Rh frame NRs from Au@Rh NRs. We first examined effects such reagent as ascorbic acid and CTAB. When prepared at higher concentrations of ascorbic acid, no significant difference in the shape of products was observed. The frame structure yield decreased (Fig. S1: ESI†). This result implies that the contribution of ascorbic acid, used as a reductant in the present system, is small for the formation of Rh nanoframe NRs. Next, we changed CTAB concentration. For example, Fig. S2 (ESI†) shows TEM images obtained at a much higher CTAB concentration of 3 M. It is noteworthy that, initially, Au@Rh NRs with shorter aspect ratios are formed at 3 h and inside Au NRs are dissolved at 6 and 9 h. This result implies that CTAB plays an important role for the formation of Rh nanoframes from Au@Rh NRs. Actually, Au NRs are known to be dissolved by the reaction of Au + $2Br^-$ oxidative etching in the presence of CTAB, O_2, and H^+.[14] Reportedly, an increase in the acid concentration enhances the Au NR oxidation rate because the addition of H^+ increases the reduction potential of the half-reaction involving O_2.[14] We found here that Au NRs are also etched at low CTAB concentration by the addition of HCl. Therefore we think that both Au + $2Br^-$ and Au + $2Cl^-$ etching reactions participate in the Au dissolution in our experiments in the presence of O_2 and H^+. Here Cl^- ions are generated from $RhCl_3 \cdot 3H_2O$. Based on the results presented above, the formation of Rh shells over Au NRs and oxidative etching of Au NRs by Br^- + O_2 occur simultaneously at high CTAB concentrations.

The one-step process described above made it difficult to control the frame morphology precisely because shell formation and oxidative etching occur simultaneously. To control the Rh frame morphology from Au@Rh NRs more easily, we separated the formation process of Rh shells over Au NRs and the oxidative etching process of Au NRs by the addition of HCl. Initially Au@Rh NRs are formed after heating reagent solution at 95 °C for 3 h. Then 6 mL of 5%HCl was added to the solution described above. It was then heated at 95 °C for 6 h. When the time evolution of products was measured by observing TEM images of products after 3, 6, and 12 h, shape changes from Au@Rh to Rh frame NRs were observed (Fig. 3). Fig. S3 (ESI†) shows a high-resolution (HR) TEM image of a typical Rh frame NR. The Rh frame exhibits clear lattice fringes indicating their poly-crystalline nature. Square lattice fringes with a lattice spacing of 0.19 nm indicate that Rh frame NRs dominantly consist of {200} facets. Fig. 4a1–4d1 and 4a2–4d2 respectively depict TEM and TEM–EDS images of Au@Rh before HCl addition and after HCl addition for 6 h. The formation of Rh frames from Au@Rh NRs was confirmed from these EDS data. The wall thickness of Rh frames was evaluated to be 5±2 nm from TEM images.

The following oxidative etching processes participates in the formation of Rh frame NRs in this two-step process.

$$\text{Au@Rh} + 2X^- (X=Br, Cl) \xrightarrow{O_2,\ H^+} \text{Rh} + AuX_2^- \quad (1)$$

To ascertain whether Au NRs used for this study are truly dissolved by the addition of Cl^- ions or not, we monitored changes in surface plasmon resonance (SPR) band of Au NRs after the addition HCl to the Au NR solution (Fig. S4: ESI†). The SPR band of Au NRs is observed in the 300–1200 nm region, with a longitudinal surface plasma resonance (LSPR) band at about 920 nm with full width at half maximum (FWHM) of about 200 nm and a weak transverse SPR band at about 510 nm. With increasing reaction time, the main peak shifts slightly from 920 nm to 880 nm because of slight shortening of Au NRs and the decreased intensity. It gives a broad band in the 800–1200 nm region without a sharp peak after 3 h. After 6 h, the SPR peak of Au NRs disappeared almost completely, which implies that Au NRs used for this study are etched oxidatively by the addition of Cl^- ions. It was therefore confirmed that etching process (1) is actually responsible for the formation of Rh frame NRs.

Fig. 5 shows SPR bands of Au NRs, Au@Rh NRs, and Rh frame NRs. When Rh shells are formed over Au NR cores, the SPR band of Au NRs decreases greatly because the SPR bands of core–shell particles generally reflect the SPR band of shell component.[15,16] When Rh frame NRs are formed, the SPR band weakens further, giving a long tail band from 300 nm to 700 nm.

To obtain information related to Au NRs, Au@Rh NRs and Rh nanoframes, powder XRD patterns were measured. Fig. 6a–6c respectively show XRD patterns of Au NRs, Au@Rh NRs, and Rh frame NRs. The XRD patterns of Au NRs indicate that the presence of the crystalline gold with fcc structure (2θ equals 38.2° and 44.4°: PDF 01-073-9564) corresponding to {111} and {200} planes. In the XRD pattern of Au@Rh obtained at an Rh/Au ratio of 5, the {111} and {200} peaks of Au become broad because of appearance of two characteristic peaks of fcc structured Rh (2θ equals 41.1° and 47.8°: PDF 00-005-0681) corresponding to {111} and {200} planes. All powder XRD data indicate that Au and Au@Rh NRs consist of fcc crystals. It is noteworthy that the Rh peaks of Au@Rh NRs shift slightly to smaller angles from standard positions of Rh, shown by vertical red lines. In addition, the Rh peaks of Au@Rh NRs become broad in comparison with those of the Au NR and Rh frame. These results indicate that the lattice constant of Rh shells change after the formation of Au@Rh NRs because of distortion of Rh shells. More significant distortion of metal shell over the same Au NR has been observed recently in Au@Pd NRs.[17] It has been explained using the lattice mismatch (4.6%) and the existence of unstable high index {2 5 0} or {5 12 0} facets in Au NRs (Fig. 7). We can find no Au–Rh alloying between Au and Rh in Au@Rh NRs prepared in EDS data. It was therefore concluded that peak shifts and broadening of Rh components in Au@Rh NRs do not arise from intermixing between Au and Rh layers. They arise from distortion of Rh lattice after formation of Au@Rh NRs.

We have prepared Rh frames using Au NRs as a sacrificial template. Actually, Au NR prepared using CTAB has long been believed to consist mainly of {100} and {110} facets.[18] The NR ends are terminated by the {100} and {111} facets with small areas. However, recent detailed studies using high-resolution TEM images and the corresponding fast Fourier transform spot patterns of Au NR have demonstrated that Au NRs comprise octagonal side-facets consisting of higher-index {2 5 0} or {5 12 0} facets.[19,20] Based on these facts, the dominant facets of Au NRs used for this study are expected to be either traditional or new {2 5 0} or {5 12 0} facets. A recent report of our earlier study discussed the crystal structures of Au NRs, which were the same as those used for this study based on TEM images of standing Au@Cu NRs.[17,21] Our Au NRs used here were round, with no sharp corners because they had bevels arising from the {110} and {100} facets between two neighbouring {2 5 0} or {5 12 0} facets, as reported by Carbó-Argibay et al.[19] and by Goris et al.[20] It is therefore concluded that our Au NRs consist of eight equivalent {2 5 0} or {5 12 0} facets and an additional eight facets of alternative {110} and {100} facets located between two {2 5 0} or {5 12 0} facets, as presented in Fig. 7.[17,21] An outstanding feature of Au NRs is that high-index {2 5 0} or {5 12 0} facets are involved in the side facets.

The formation mechanism of Rh nanoframe is portrayed in Fig. 7. A large lattice mismatch (6.8%) occurs between fcc Au (lattice constant = 0.4080 nm) and Rh (0.3803 nm). In addition, Au NRs have unstable high index facets such as {2 5 0} or {5 12 0}. Therefore, layered growth of Rh shell over Au NR is difficult and island-type Rh particles are grown over Au NRs. When HCl was added in the presence of CTAB, X^- (X=Br, Cl) ions, and O_2 dissolved in the reagent solution penetrate into the interspace and Au NRs are oxidatively etched through the

reaction (1). It is noteworthy that hollow structures are not formed but Rh nanoframes are formed. Based on TEM images obtained from different angles (Fig. S5, ESI†), Rh nanoframes consist of four side edges and top and bottom edges. Therefore, the remaining Rh frames arise with either four {100} or {110} side facets and side {100} facets because eight edge frames will remain, if Rh particles on the {2 5 0} or {5 12 0} facets remain after etching (see side view of Au NR in Fig. 7). During etching of Au core NR, Rh island shells are also etched by X^- (X = Br, Cl) and O_2. However, the etching rate depends strongly on the underlying facets of Au. HRTEM images indicate that Rh nanoframes dominantly consist of the {100} facet. On the basis of this fact, it is reasonable to assume that the Rh particles on unstable {110} and {2 5 0} or {5 12 0} facets are etched, whereas those on stable {100} facet are not dissolved by the addition of HCl. Therefore Rh frame NRs having four bridges are formed. Although Au has superior chemical stability compared to many other metals, Au NRs are etched preferentially from Au@Rh NRs due to the better surface passivation of Rh by CTAB and/or the relatively high stability of Rh toward Au NRs. Similar preferential etching of metallic Au has been reported in the cases of Au@Pt particles leading to various shapes of Pt frames, although responsible etching processes are different from each other.[22-24]

Decahedral Au@Rh nanoparticles produced from Au decahedra as seeds

To examine the formation mechanism of Rh nanoframes, we examined the effects of morphologies of Au cores for the formation of Rh nanoframes using decahedral Au seeds. Rh^{3+} ions were reduced in the presence of decahedral Au cores under the same experimental conditions as those used for Rh frames from Au@Rh NRs. Fig. 8a shows typical TEM and TEM–EDS images of decahedral Au@Rh nanoparticles before HCl addition. Smoother Rh shells than those on Au NRs are formed; although Rh shells do not form layered structures, they are covered by small spherical island-type Rh particles.

When examining oxidative etching of Au decahedral particles by the addition of HCl, they are dissolved as in the case of Au NRs (Fig. S6, ESI†). That dissolution indicates that decahedral Au nanoparticles can be etched as in the case of Au NRs by the addition of HCl. We have examined whether frame structures are formed after addition of the same amount of HCl as that used for the preparation Rh frame from Au@Rh NRs. It is noteworthy that no frame structure can be formed as presented in Fig. 8b. Two possible reasons can explain the absence of frame formation. One is the lack of interspace in Rh layers because decahedral Au particles are covered by rather smooth Rh shells. Another reason is that Rh shells over low index {111} facets are too stable to be etched. No peak shifts caused by lattice distortion were observed in decahedral Au@Rh particles (Fig. S7, ESI†). Therefore, no frame structure is formed from decahedral Au@Rh nanoparticles (Fig. 8b). Based on the facts presented above, it can be concluded that unstable high index facets play important roles in frame structure formation.

Conclusion

Formation of Rh frame NRs was examined using Au NRs as sacrificial template. Two formation processes are possible for the formation of Rh nanoframes. One is a one-step process in which Au@Rh NRs were formed initially in the presence of ascorbic acid and CTAB. Then Au core parts were dissolved by $Au + 2X^-$ (X = Br, Cl) reaction in the presence of O_2 and H^+ with increasing the reaction time. Finally, the Rh frame NRs are formed by oxidative etching of Au NRs and Rh shells over unstable {110} and {2 5 0} or {5 12 0} facets of Au NRs. Another process is two-step process in which Au@Rh was initially prepared in the presence of ascorbic acid and CTAB. Then Au and Rh over {110} and {2 5 0} or {5 12 0} facets were etched by the addition of HCl. To clarify why preferential etching of Au NRs and face selective etching of Rh frames occur in our conditions, further detailed experimental studies on the roles of each etchant and surfactant will be required.

To obtain information related to effects of shape of Au core for the formation of Rh nanoframe, decahedral Au@Rh was prepared. Then HCl was added for the frame structure formation. No frame structure was formed after the HCl addition, as explained by the smooth Rh shells over decahedral Au core and slow etching rate of low-index {111} facets. Results obtained in this study suggest a new synthesis method at the low reaction temperature of 95 °C in an aqueous solution and an Rh nanoframe growth mechanism from Au@Rh NRs.

Acknowledgements

We thank Dai Nippon Toryo Co., Ltd. for supplying Au NRs. This work was supported by JSPS KAKENHI (grant nos. 25286003 and 25550056) and by Management Expenses Grants for National University Corporations from MEXT.

Notes and references

[a] Institute for Materials Chemistry and Engineering, Kyushu University, Kasuga 816-8580, Japan. E-mail: tsuji@cm.kyushu-u.ac.jp; Fax: +81 092 583 7815; Tel.: +81 092 583 7815
[b] Department of Applied Science for Electronics and Materials, Graduate School of Engineering Sciences, Kyushu University, Kasuga 816-8580, Japan
[c] Department of Automotive Science, Graduate School of Integrated Frontier Sciences, Kyushu University, Kasuga, 816-8580, Japan

† Electronic Supplementary Information (ESI) available: [additional TEM, HRTEM, UV–Vis–NIR, and XRD data]. See DOI: 10.1039/b000000x/

1 S. W. Kim, M. Kim, W. Y. Lee and T. Hyeon, *J. Am. Chem. Soc*., 2002, **124**, 7642.
2 Y. G. Sun, B. Mayers and Y. Xia, *Adv. Mater*., 2003, **15**, 641.
3 S. E. Skrabalak, J. Chen, Y. Sun, X. Lu, L. Au, C. M. Cobley, and Y. Xia, *Acc. Chem. Res*., 2008, **41**, 1587.
4 C. M. Cobley and Y. Xia, *Mater. Sci. Eng. R.*, 2010, **70**, 44.
5 X. Xia, Y. Wang, A. Ruditskiy and Y. Xia, *Adv. Mater*., 2013, **25**, 6313.
6 M. Tsuji, T. Kidera, A. Yajima, M. Hamasaki, M. Hattori, T. Tsuji and H. Kawazumi, *CrystEngComm*, 2014, **16**, 2684.

7 M. Tsuj, M. Hamasaki, A. Yajima, M. Hattori, T. Tsuji and H. Kawazumi, *Mater. Lett*., 2014, **121**, 113.
8 Y. G. Sun and Y. Xia, *J. Am. Chem. Soc*., 2004, **126**, 3892.
9 Y. G. Sun and Y. Xia, *Adv. Mater*., 2004, **16**, 264.
10 Y. G. Sun, B. Wiley, Z.-Y. Li and Y. Xia, , *J. Am. Chem. Soc*., 2004, **126**, 9399.
11 Y. Niidome, Y. K. Nishioka, H. Kawasaki and S. Yamada, *Chem. Commun*. 2003, 2376.
12 D. Seo, C. I. Yoo, I. S. Chung, S. M. Park, S. Ryu and H. Song, *J. Phys. Chem. C*, 2008, **112**, 2469.
13 M. Tsuji, N. Nakamura, M. Ogino, K. Ikedob and M. Matsunaga, *CrystEngComm*, 2012, **14**, 7639.
14 C.-K. Tsung, X. Kou, Q. Shi, J. Zhang, M. H. Yeung, J. Wang and G. D. Stucky, *J. Am. Chem. Soc*., 2006, **128**, 5352.
15 M. B. Cortie and A. M. McDonagh, *Chem. Rev*., 2011, **111**, 3713.
16 M. Tsuji, K. Ikedo, K. Uto, M. Matsunaga, Y. Yoshida, K. Takemura and Y. Niidome, *CrystEngComm*, 2013, **15**, 6553.
17 M. Tsuji, K. Takemura, C. Shiraishi, K. Ikedo, K. Uto, A. Yajima, M. Hattori, Y. Nakashima, K. Fukutomi, K. Tsuruda, T. Daio, T. Tsuji and S. Hata, *J. Phys. Chem. C*, 2015, in press, DOI: 10.1021/jp509340s.
18 Z. L. Wang, M. B. Mohamed, S. Link and M. A. El-Sayed, *Surf. Sci*., 1999, **440**, L809.
19 E. Carbó-Argibay, B. Rodríguez-González, S. Gómez-Graña, A. Guerrero-Martínez, I. Pastoriza-Santos, J. Pérez-Juste and L. M. Liz-Marzán, *Angew. Chem., Int. Ed.,* 2010, **49**, 9397.
20 B. Goris, S. Bals, W. Van den Broek, E. Carbó-Argibay, S. Gómez-Graña, L. M. Liz-Marzán and G. Van Tendeloo, *Nat. Mater*., 2012, **11**, 930.
21 Y. Yoshida, K. Uto, M. Hattori, and M. Tsuji, *CrystEngComm*, 2014, **16**, 5672.
22 M. Min, C. Kim, Y. I. Yang, J. Yib and H. Lee, *Chem. Commun*., 2011, **47**, 8079.
23 N. Fan, Y. Yang, W. Wang, L. Zhang, W. Chen, C. Zou and S. Huang, *ACS Nano*, 2012, **6**, 4072.
24 H.-J. Jang, S. Ham, J. A. I. Acapulco, Jr., Y. Song, S. Hong, K. L. Shuford and S. Park, *J. Am. Chem. Soc*., 2014, **136**, 17674.

Graphical Abstract

Formation of Rh frame nanorods was studied using Au nanorods having high index facets as sacrificial template.

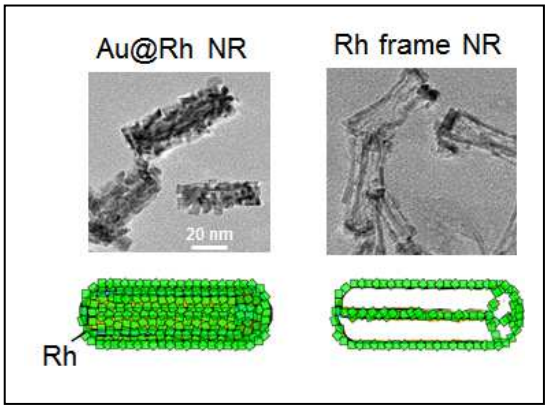

Figure captions

Fig. 1. TEM images of Au NRs, Au@Rh NRs, and Rh frames obtained after 3, 6, 9, and 12 h.

Fig. 2. TEM and TEM-EDS images of Au@Rh NRs obtained after (a) 3 h and (b) 12 h.

Fig. 3. TEM images of Au@Rh NRs and Rh frame NRs obtained after 3, 6, and 12 h.

Fig. 4. TEM and TEM-EDS images of (a) Au@Rh NRs obtained before HCl addition and (b) Rh frame NRs obtained after HCl addition for 6 h.

Fig. 5. SPR bands of Au NRs Au@Rh NRs, and Rh frame NRs.

Fig. 6. XRD patterns of Au NRs, Au@Rh NRs, and Rh frame NRs. Red lines show standard positions of Rh peaks.

Fig. 7. Formation mechanism of Rh frame NR from Au and Au@Rh NRs in the presence of CTAB and HCl.

Fig. 8. TEM and TEM–EDS images of decahedral Au@Rh nanoparticles (a) before and (b) after HCl addition for 12 h.

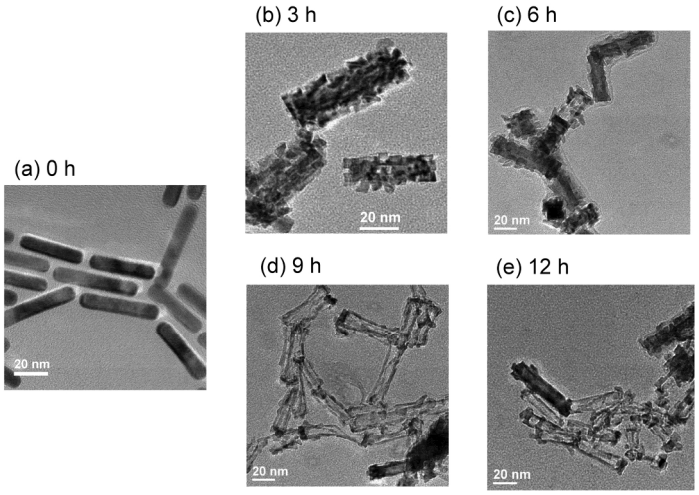

Fig. 1 M. Tsuji et al.

209x148mm (300 x 300 DPI)

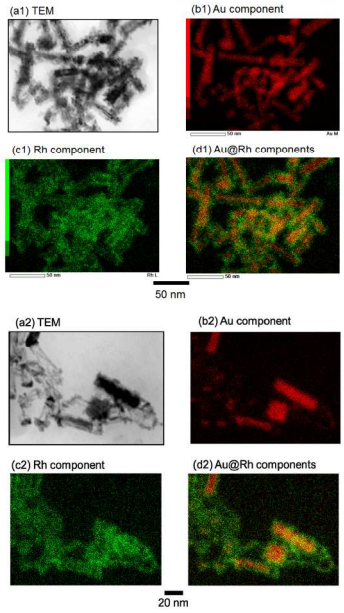

Fig. 2 M. Tsuji et al.

209x148mm (300 x 300 DPI)

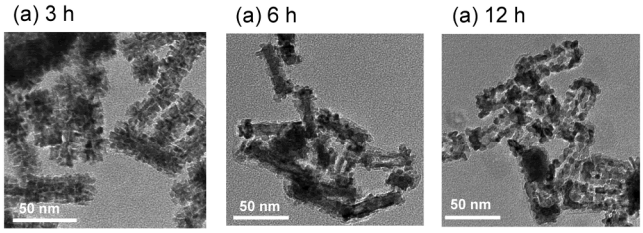

Fig. 3 M. Tsuji et al.

209x148mm (300 x 300 DPI)

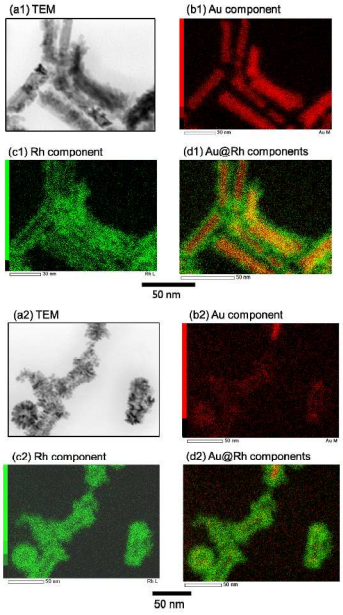

Fig. 4 M. Tsuji et al.

297x210mm (300 x 300 DPI)

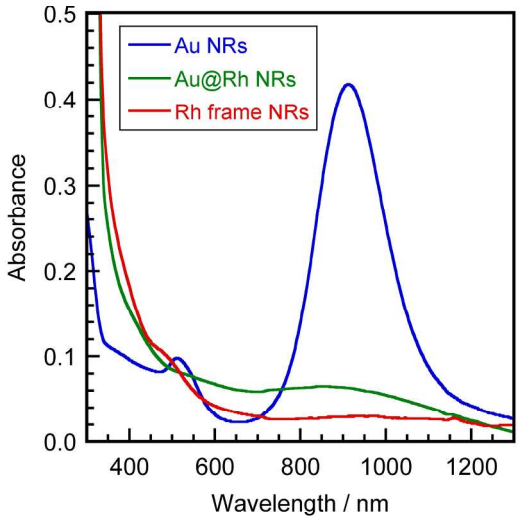

Fig. 5 M. Tsuji et al.

209x148mm (300 x 300 DPI)

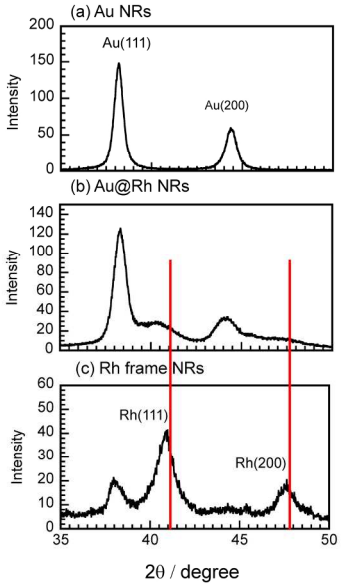

Fig. 6 M. Tsuji et al.

209x148mm (300 x 300 DPI)

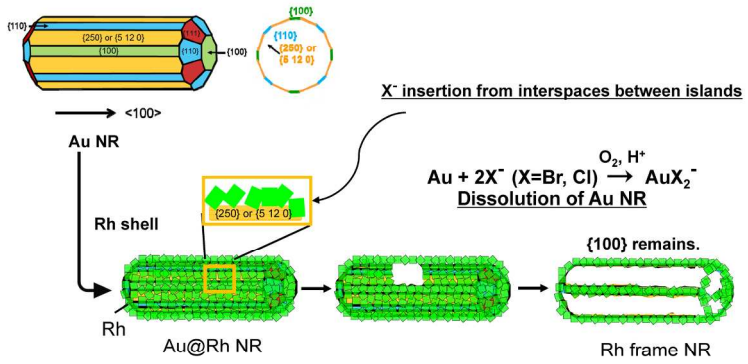

Fig. 7 M. Tsuji et al.

209x148mm (300 x 300 DPI)

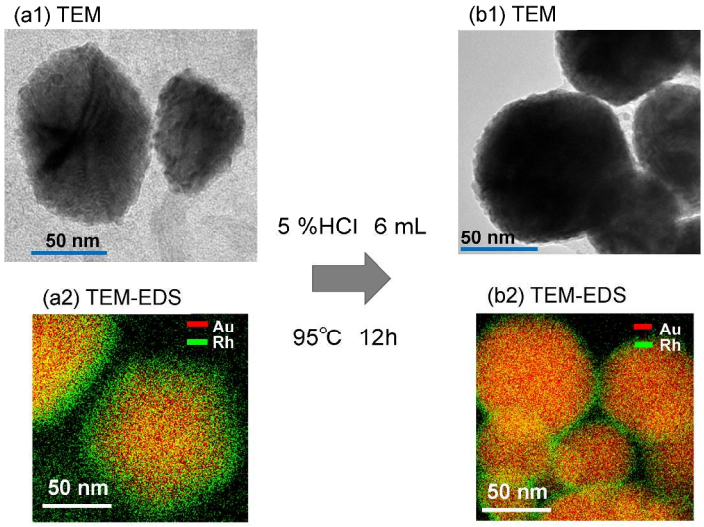

Fig. 8 M. Tsuji et al.

297x210mm (300 x 300 DPI)